Ion Bernstein Wave Heating in a Multi-Component Plasma

Satish Puri

IPP 4/193 October 1980

MAX-PLANCK-INSTITUT FÜR PLASMAPHYSIK

8046 GARCHING BEI MÜNCHEN

MAX-PLANCK-INSTITUT FÜR PLASMAPHYSIK

GARCHING BEI MÜNCHEN

Ion Bernstein Wave Heating in a Multi-Component Plasma

Satish Puri

IPP 4/193 October 1980

Die nachstehende Arbeit wurde im Rahmen des Vertrages zwischen dem Max-Planck-Institut für Plasmaphysik und der Europäischen Atomgemeinschaft über die Zusammenarbeit auf dem Gebiete der Plasmaphysik durchgeführt.

ION BERNSTEIN WAVE HEATING IN A MULTI-COMPONENT PLASMA

Satish Puri

Max-Planck-Institut für Plasmaphysik

D-8046 Garching, FRG

Abstract

Conditions for the coupling and absorption of Gross-Bernstein ion-cyclotron waves in a multi-component plasma are examined. Two cases are distinguished depending upon whether, the antenna initially launches, (i) the quasi-torsional slow electromagnetic wave with azimuthal magnetic field (TM) polarization, or (ii) the quasi-compressional fast wave with the electric field oriented azimuthally (TE). Analytic expressions for the plasma surface impedance are derived taking into account the pertinent warm plasma modifications near the vacuum-plasma interface. Antenna configurations capable of efficient coupling of the radio frequency energy to these modes are studied. A method for simulating waveguide like launching using transmission lines is pointed out. It is found that impurity concentrations exceeding a few parts in a thousand are capable of competing with the bulk ions in the energy absorption processes; this could lead to energy deposition near the plasma edge. Measures for avoiding edge heating problems by a careful choice of parameters e.g. restricting the heating frequency to the fundamental ion gyrofrequency are outlined. Equal care is to be exercised in limiting the n_z spectrum to low descrete values in order to avoid the potentially dangerous problem of run-away electron heating.

1. INTRODUCTION

We have earlier described (PURI and TUTTER, 1975; PURI, 1975, 1978, 1979) a plasma heating method using Gross-Bernstein (GROSS, 1952; BERNSTEIN, 1958) ion-cyclotron waves employing the coupling techniques of the lower-

hybrid wave heating. This heating scheme derives its appeal from among others, (i) the ease of accessibility, (ii) possibility of direct ion heating, (iii) insensitiveness of the energy deposition occuring near the plasma core to variations in density or temperature of the plasma, (iv) feasibility of waveguide coupling in the manner of lower-hybrid heating (KARNEY et al, 1973; LALLIA, 1974; BRAMBILLA, 1976). Recent theoretical results (ONO et al, 1979, 1980 a, 1980 b; PURI, 1980) as well as the experimental verification (ONO, 1980 c) of this concept uphold this optimism.

In this paper, the Gross-Bernstein wave heating results are extended to the case of a multi-component plasma. Although the available choice of plasma and magnetic field parameters permits a rich palette of possibilities, we limit the treatment to three examples. In all of these instances, the externally launched electromagnetic wave merges (through successive wave transformations) with the Gross-Bernstein wave as it traverses continuously connected zones of propagation except, perhaps, a thin envanescent region near the plasma edge.

The first two cases involve the slow (s) electromagnetic mode which transforms successively into the electron-plasma (p) wave and the electrostatic Bernstein (e) wave, respectively, on its encounter with the lower-hybrid (LHR) and the Buchsbaum hybrid (BHR) resonances, respectively. The third case involves the excitation of the fast (f) electromagnetic mode which after conversion to the s wave at the cold-plasma confluence (see sec. 2.2), transforms to the p and e waves near the BHR. The e waves are eventually assimilated through a combination of ion-cyclotron damping (ICD) and electron-Landau damping (ELD) in a hot thermonuclear plasma (PURI, 1979). For convenience we will refer to these three cases as (i) the lower-hybrid Gross-Bernstein (LHGB) heating, (ii) the Buchsbaum-hybrid Gross-Bernstein (BHGB) heating and (ii) the fast wave Gross-Bernstein (FWGB) heating, respectively. The general qualitative appearance of the dispersion characteristics of these

modes in a torus machine is shown in Fig. 1. Following a description of the plasma model in Sec. 2. each of these modes is treated in detail in Secs. 3, 4, and 5, respectively.

2. THE PLASMA MODEL

2.1 The Geometry

The torus plasma is simulated by the flattened slab representation of Fig. 2. This simplification, while retaining the essential physics, allows mathematical tractability. We assume a linear density profile peaked at $x = 0$, a uniform temperature T and the validity of the local dielectric tensor. The static magnetic field is B_0 on the axis ($x = 0$), $B_0 (1+\mathcal{A}^{-1})^{-1}$ at the outer plasma radius ($x = a$) and $B_0 (1+\mathcal{A}^{-1})$ at the inner plasma radius ($x = -a$), where $\mathcal{A}$ is the torus aspect ratio, R/a. The plasma is contained within perfectly conducting walls at $x = \pm c$. The radio frequency power is coupled using either ideal current carrying antennas at $x = \pm b$ or by electric field gaps in the walls. Under certain conditions, a Faraday shield with an anisotropic conductivity ($\sigma_y = 0$, $\sigma_z = \infty$) may be required between the plasma and the antenna at $x = -f$. Since a finite k_y is not essential to the physical processes involved, all field quantities are assumed to vary as $\exp i(k_z z - \omega t)$.

Departures from ideal conditions such as a non-uniform temperature profile, finite wall conductivity or steeper density profiles are made where appropriate.

2.2 Cold Plasma Dispersion

For a fixed parallel refractive index $n_z = c\, k_z/\omega$, the cold plasma dispersion relation may be expressed as

$$A\, n_x^4 - B\, n_x^2 + C = 0, \qquad (2.1)$$

where

$$A = \epsilon_x \,, \tag{2.2}$$

$$B = \epsilon_z (\epsilon_x - n_z^2) + \epsilon_L \epsilon_R - \epsilon_x n_z^2 \,, \tag{2.3}$$

$$C = \epsilon_z (\epsilon_L - n_z^2)(\epsilon_R - n_z^2) \,, \tag{2.4}$$

$$\epsilon_x = 1 - \sum_j \frac{\omega_{pj}^2}{\omega^2 - \omega_{cj}^2} \,, \tag{2.5}$$

$$\epsilon_y = -i \sum_j s_j \frac{\omega_{cj}}{\omega} \frac{\omega_{pj}^2}{\omega^2 - \omega_{cj}^2} \,, \tag{2.6}$$

$$\epsilon_z = 1 - \sum_j \frac{\omega_{pj}^2}{\omega^2} \,, \tag{2.7}$$

$$\epsilon_L = 1 - \sum_j \frac{\omega_{pj}^2}{\omega^2} \frac{\omega}{\omega - s_j \omega_{cj}} \,, \tag{2.8}$$

$$\epsilon_R = 1 - \sum_j \frac{\omega_{pj}^2}{\omega^2} \frac{\omega}{\omega + s_j \omega_{cj}} \,, \tag{2.9}$$

and $s_j = \pm 1$ is the sign of the charge of the particle of the j^{th} species. We will have the occasion to employ the useful relations,

$$\epsilon_R = \epsilon_x + i \epsilon_y \tag{2.10}$$

$$\epsilon_L = \epsilon_x - i \epsilon_y \tag{2.11}$$

and

$$\epsilon_L \epsilon_R = \epsilon_x^2 + \epsilon_y^2 \,. \tag{2.12}$$

Critical phenomena are associated with the zeros of A, $\mathcal{D} = B^2 - 4AC$, and C. Thus C vanishes at the plasma cutoff $\epsilon_z = 0$, the left cutoff

$\epsilon_L = n_z^2$, and the right cutoff $\epsilon_R = n_z^2$. The zero of the discriminant D implies a confluence or a double root where the s and the f waves merge. Various hybrid resonances, one between each adjecent pair of cyclotron resonances ($n_x \to \infty$), occur when $A \to 0$. Near these resonances, the perpendicular wave length λ_x is no longer large compared to the particle gyroradii, so that the cold-plasma approximation breaks down and one is obliged to use the hot-plasma description. Other situations requiring hot-plasma treatment occur due to the onset of ELD when the electron thermal velocity, v_{ze} becomes comparable to the wave phase velocity, v_{pz} along the static magnetic field direction.

2.3 Hot Plasma Dispersion

Assuming $v_{ze} / c \ll 1$, the hot-plasma dielectric tensor components may be written as (PURI, 1979),

$$\epsilon_x = 1 + \sum_j \frac{\omega_p^2}{\omega \omega_c} \zeta_0 \frac{e^{-\Lambda}}{\Lambda} \sum_{-\infty}^{\infty} n I_n(\Lambda) Z_n , \qquad (2.13)$$

$$\epsilon_y = i \sum_j s_j \frac{\omega_p^2}{\omega \omega_c} \zeta_0 e^{-\Lambda} \sum_{-\infty}^{\infty} I_n'(\Lambda) Z_n , \qquad (2.14)$$

and

$$\epsilon_z = 1 + \sum_j \frac{\omega_p^2}{\omega^2} \zeta_0^2 e^{-\Lambda} \sum_{-\infty}^{\infty} I_n(\Lambda) Z_n' , \qquad (2.15)$$

where I_p is the modified Bessel function, Z_n is the plasma dispension function defined by

$$Z_n = Z(\zeta_n) = -i \pi^{1/2} \exp(-\zeta_n^2) + \pi^{1/2} \int_{-\infty}^{\infty} \frac{\exp(-t^2)\, dt}{t - \zeta_n} , \quad \mathrm{Im}\, \zeta_n > 0 , \qquad (2.16)$$

$$\zeta_n = \frac{\omega - n\omega_c}{k_z v_z} = \frac{c}{n_z v_z} \left(1 - \frac{n\omega_c}{\omega}\right) , \qquad (2.17)$$

$\Lambda = (1/2) k_x^2 r_c^2$, $Z_n' = \partial Z_n / \partial \zeta_n$ and $I_n' = \partial I_n / \partial \Lambda$.

Wherever unambiguous from context, the subscript j has been omitted in the above equations.

Frequently, one encounters situations where Λ, though finite, is small. Upon retaining only the lowest order terms in the series expansion of $\underline{\underline{\epsilon}}$ in Λ, the most significant warm-plasma modification occurs in ϵ_x which becomes,

$$\epsilon_x = \epsilon_x^c + \sum_j \Lambda \left(\frac{\omega_p^2}{\omega^2 - \omega_c^2} - \frac{\omega_p^2}{\omega^2 - 4\omega_c^2} \right), \quad (2.18)$$

where ϵ_x^c is the cold-plasma contribution.

3. LOWER HYBRID GROSS-BERNSTEIN HEATING

3.1 The Dispersion Characteristics

For the case when the antenna is located at the outer torus circumference and $\omega_{ce} > \omega > \omega_{cj}$ for all ionic species j, $\epsilon_x \to 0$ at the lower hybrid resonance. Fig. 3 shows the computed dispersion characteristics of the lower-hybrid wave in the presence of simultaneous density and magnetic field gradients. The curves for a D-e plasma were obtained using the full hot plasma dielectric tensor described in Sec. 2.3. After complete conversions (STIX, 1965) to p and e, respectively, the wave encounters the ion-cyclotron resonance (ICR) where it is completely assimilated without reflection (PURI, 1978, 1979). In addition, for larger T_e and n_z such that $\zeta_{oe} \sim O(1)$, additional absorption occurs through ELD.

The above essential features are retained in a multi-component plasma. A fresh series of ion-cyclotron-harmonic resonances with corresponding dispersion curves is introduced by each particle species with a different

charge to mass ratio. Following the first wave conversion whose location depends upon the plasma parameters, the wave is absorbed by the ICR closest to conversion region on the high magnetic field side. Further complications introduced by the presence of impurities or minority species are covered in Sec. 3.6.

3.2 Cold Plasma Accessibility and Impedance

The Golant accessibility condition (GOLANT, 1971)

$$n_z^2 \gtrsim 1 + \frac{\omega_{pe}^2}{\omega_{ce}^2} \qquad (3.1)$$

may be expressed as (PURI and TUTTER, 1975),

$$n_z^2 \gtrsim 1 + \frac{m_e}{f_k m_k} \frac{\omega_{pk}^2}{\omega_{ck}^2}$$

$$\gtrsim 1 + \frac{m_e}{f_k m_k} \frac{1}{\omega_{ck}^2} \left(\omega_{LH}^2 - \sum_{j \neq k} \omega_{pj}^2 \right). \qquad (3.2)$$

In obtaining (3.2) it was assumed that $\omega_{LH}^2 \simeq \Sigma\, \omega_{pj}^2$, where the summation extends over all the ionic species. The inequality (3.2) holds if,

$$n_z^2 \gtrsim 1 + \frac{1}{f_k} \frac{m_e}{m_k} N_k^2 \,, \qquad (3.3)$$

where $N_k = \omega_{LH}/\omega_{ck}$ and f_k is the fractional contribution of the k_{th} ionic species. For $N_k \ll (m_k/m_e)^{1/2} f_k^{1/2}$, accessibility occurs at the rather undemanding condition $n_z \sim 1$. Ease of accessibility was part of the rationale which originally led us to propose plasma heating at the low ion-cyclotron harmonics. In Sec. 3.3 we will see that still more favourable conditions for accessibility occur for coupling at these low frequencies when the warm plasma effects are incorporated in the model. For low

$N_k \sim O(1)$ even though the approximation $\omega_{LH} \simeq \omega_{pi}$ used for obtaining (3.2) is no longer valid, the above conclusions continue to hold because of the negligible contribution from the final term in (3.3).

The case for which (3.3) is satisfied, n_x in (2.1) is real everywhere between the LHR and the plasma boundary excepting an insignificant region near the edge for which $\omega_{pe} < \omega$ and $\epsilon_z > 0$. The differential equations governing the lower-hybrid propagation near the plasma edge may be obtained from the Maxwell's equations in the form (GOLANT, 1971),

$$\frac{\partial^2 E_z}{\partial x^2} + \frac{1}{\epsilon_x} \frac{n_z^2}{n_z^2 - \epsilon_x} \frac{\partial \epsilon_x}{\partial x} \frac{\partial E_z}{\partial x} + (\epsilon_x - n_z^2) \frac{\epsilon_z}{\epsilon_x} E_z = 0, \quad (3.4)$$

and

$$H_y = \frac{1}{i\eta} \frac{\epsilon_x}{n_z^2 - \epsilon_x} \frac{\partial E_z}{\partial x}, \quad (3.5)$$

where $x = k_o x$. Introducing, $\epsilon_x' = \partial \epsilon_x / \partial x$ and

$$\mathcal{E}_z = \left(\frac{\epsilon_x}{n_z^2 - \epsilon_x} \right)^{1/2} E_z, \quad (3.6)$$

in (3.4), one obtains upon neglecting terms containing ϵ_x'',

$$\frac{\partial^2 \mathcal{E}_z}{\partial x^2} - \left[(n_z^2 - \epsilon_x) \frac{\epsilon_z}{\epsilon_x} - \frac{1}{4} \frac{\epsilon_x'^2}{\epsilon_x^2} \frac{n_z^2 - 4\epsilon_x}{(n_z^2 - \epsilon_x)^2} \right] \mathcal{E}_z = 0. \quad (3.7)$$

Assuming

$$|\epsilon_z| >> \left| \frac{\epsilon_x'^2}{4\epsilon_x} \frac{n_z^2 - 4\epsilon_x}{(n_z^2 - \epsilon_x)^3} \right|, \quad (3.8)$$

(3.7) simplifies to

$$\frac{\partial^2 \mathcal{E}_z}{\partial x^2} - (n_z^2 - \epsilon_x) \frac{\epsilon_z}{\epsilon_x} \mathcal{E}_z = 0. \quad (3.9)$$

The assumption (3.8) is readily satisfied in the practical cases of inter-

est occuring in Sec. 3.3.

Treating the slowly varying ϵ_x constant in comparison with ϵ_z, we may write (3.9) as

$$\frac{\partial^2 \epsilon_z}{\partial \xi^2} + \psi^2 \xi \epsilon_z = 0 , \tag{3.10}$$

where

$$\xi = x - u_z , \tag{3.11}$$

$$\psi^2 = \frac{n_z^2 - \epsilon_x}{u_z \epsilon_x} \tag{3.12}$$

and

$$u_z = - \left(\frac{\partial \epsilon_z}{\partial x} \right)^{-1} . \tag{3.13}$$

Equation (3.10) has the Hankel function solution

$$\mathcal{E}_z = p \xi^{1/2} H^{(1)}_{1/3} \left(\tfrac{2}{3} \psi \xi^{3/2} \right) + q \xi^{1/2} H^{(2)}_{1/3} \left(\tfrac{2}{3} \psi \xi^{3/2} \right) , \tag{3.14}$$

with the asymptotic form,

$$\mathcal{E}_z \sim p \left(\tfrac{3}{\pi}\right)^{1/2} \xi^{-1/4} e^{i\left(\frac{2}{3}\psi\xi^{3/2} - \frac{5\pi}{12}\right)} + q \left(\tfrac{3}{\pi}\right)^{1/2} \xi^{-1/4} e^{-i\left(\frac{2}{3}\psi\xi^{3/2} - \frac{5\pi}{12}\right)} . \tag{3.15}$$

The absence of a returning wave from the plasma interior implies $p \equiv 0$ for the backward s wave. To simplify later algebraic manipulations, it is advantageous to replace the Hankel function $H^{(2)}_{1/3}$ in (3.14) by Bessel functions, giving

$$\mathcal{E}_z = q \xi^{1/2} \left[J_{-1/3} \left(\tfrac{2}{3} \psi \xi^{3/2} \right) - e^{-\frac{n i}{3}} J_{1/3} \left(\tfrac{2}{3} \psi \xi^{3/2} \right) \right] , \tag{3.16}$$

which for small argument $(2/3)\psi\xi^{3/2}$ valid near the plasma edge yields using (3.6) and (3.5),

$$E_z = q \left[\frac{1}{\Gamma(\frac{2}{3})} \left(\frac{\psi}{3} \right)^{-1/3} - e^{\frac{\pi i}{3}} \frac{1}{\Gamma(\frac{4}{3})} \left(\frac{\psi}{3} \right)^{1/3} \xi \right] \left(\frac{n_z^2 - \epsilon_x}{\epsilon_x} \right)^{1/2} , \tag{3.17}$$

and $$H_y = -\frac{1}{i\eta}\left(\frac{\epsilon_x}{n_z^2-\epsilon_x}\right)^{1/2} e^{\pi i/3}\frac{1}{\Gamma(\frac{4}{3})}\left(\frac{\psi}{3}\right)^{1/3} . \quad (3.18)$$

Finally the normalized surface impedance $\sigma_s = iE_z/\eta H_y$ is given by

$$\sigma_s = s\, e^{-\pi i/3}\, u_z^{1/3}\left(\frac{n_z^2-\epsilon_x}{\epsilon_x}\right)^{2/3} \quad (3.19)$$

where,

$$s = 3^{2/3}\,\Gamma(\tfrac{4}{3})/\Gamma(\tfrac{2}{3}) . \quad (3.20)$$

Except for an algebraic correction by a factor of one half, (3.19) is the result obtained by Golant (GOLANT, 1971).

Let us recount some of the assumptions used in obtaining (3.19):

(i) The plasma possesses a strictly linear profile so that $u_z = -(\partial\epsilon_z/\partial x)^{-1}$ is precisely defined. In practice, a tenous plasma (promoting propagating conditions) extends from the antenna till the shadow of the limiter; while uncertain and changing density gradients exist beyond the limiter. Since σ_s varies as one-third power of u_z, a crude but acceptable method for defining u_z may consist in replacing it by the averaged value $\langle u_z\rangle = -\langle\partial\epsilon_z/\partial x\rangle^{-1}$. The averaging distance should extend over the region where the WKB conditions are violated and wave reflections continue to occur. It may be prudent to exclude the propagating region between the antenna and the limiter shadow from this averaging because the weak density gradients, in fact, promote WKB like conditions. Thus, a reasonable guideline may be to perform the averaging over a distance of $O(\langle\lambda_x\rangle)$ defined by,

$$\int_{x_L}^{x_L+\langle\lambda_x\rangle} k_x(x)\,dx = 1 , \quad (3.21)$$

where, x_L is the location of the limiter shadow in the vicinity of the antenna.

(ii) the next crucial assumption involves treating $\epsilon_x \sim 1$ near the edge. This is true for the usual lower-hybrid heating schemes in which the LHR is well removed from the edge and WKB conditions prevail before any significant change in the value of ϵ_x occurs. In the present context, however, the cold-plasma LHR occurs at $n_e \sim 0$ (10^{10} cm^{-3}), the LHR may be altogether absent and $\epsilon_x \ll 1$ close to the antenna surface. Consequently $n_x \gg 1$ in (2.1), Λ is no longer vanishingly small and the finite gyroradius effects assume significance. In the following section the modifications introduced by the warm plasma effects are studied.

3.3 Warm Plasma Impedance and Accessibility

As was mentioned in Sec. 2.3, the lowest order temperature correction involves replacing the cold plasma ϵ_x by its warm plasma counterpart. From (2.18),

$$\epsilon_x = \epsilon_x^c + \Lambda_k \mathcal{S}_i \,, \tag{3.22}$$

where,

$$\mathcal{S}_i = \sum_j \frac{m_j}{m_k} \left(\frac{\omega_{pj}^2}{\omega^2 - \omega_c^2} - \frac{\omega_{pj}^2}{\omega^2 - 4\omega_{cj}^2} \right). \tag{3.23}$$

Also from (2.1), using $q = \epsilon_z(\epsilon_x - n_z^2)$ and $n_x \gg 1$,

$$n_x^2 \simeq -\frac{\epsilon_z}{\epsilon_x}(n_z^2 - \epsilon_x) \,, \tag{3.24}$$

for the slow wave. At the location of the LHR, since $\epsilon_x^c = 0$ and $\epsilon_x \ll 1$,

$$n_x^2 = \left(\frac{-2\epsilon_z n_z^2}{k_o^2 r_{ck}^2 \mathcal{S}_i} \right)^{1/2} \tag{3.25}$$

and

$$\Lambda_k = \tfrac{1}{2} k_o^2 r_{ck}^2 n_x^2 \,. \tag{3.26}$$

From (3.22) to (3.26),

$$n_x^2 \simeq \frac{10^5 A_i^{1/2} n_z (-2\epsilon_z)^{1/2}}{\pi T_i^{1/2} S_i^{1/2}} \tag{3.27}$$

$$k_x^2 \simeq \frac{10^{-9} \pi n_z B_o^2 (-2\epsilon_z)^{1/2}}{A_i^{3/2} S_i^{1/2} T_i^{1/2}} \tag{3.28}$$

$$\Lambda_k \simeq \frac{5\times 10^{-6} \pi n_z T_i^{1/2} (-2\epsilon_z)^{1/2}}{A_i^{1/2} S_i^{1/2}} \tag{3.29}$$

where, A_i is measured in proton mass units, B_o in Gauss and T_e in eV. For $-\epsilon_z \sim \omega_{pe}^2/\omega^2 \sim \omega_{pe}^2/\omega_{pi}^2 \sim O(m_i/m_e)$, $S_i \sim O(1)$, $A_i \sim O(2)$, $T_i \sim O(100 eV)$, and $B_o \sim O(75 kG)$, one arrives at the estimates $\epsilon_x \sim \Lambda_k \sim O(10^{-2} n_z^2)$, $n_x \sim O(6 n_z)$, and $\lambda_x \sim O(n_z^{-1/2}\ cm)$ at the location of the LHR.

As the wave travels further, $\epsilon_x \sim (1/2) k_o^2 r_c^2 n_z^2 S_i \epsilon_z / \epsilon_x^c$ changes gradually till the wave becomes electrostatic and $\epsilon_x \to 0$. Simultaneously, the wavelength λ_x shortens and presently becomes small compared to the gradient length, so that the WKB conditions are applicable and the wave progresses without further reflection. The observations pertinent to further analytical development may now be summarized as:

(i) The region separating the antenna surface and the cold-plasma LHR is either altogether absent or is optically so thin that $\int k_x dx \ll 1$ and complete transmission occurs.

(ii) $\epsilon_x \sim O(10^{-2})$ may be assumed constant near the plasma edge. As such the surface impedance result of (3.19) continues to be valid.

Observe the dramatic increase in the plasma surface impedance by a factor of over twenty compared to its cold plasma value. For $\epsilon_x \sim O(10^{-2})$ and $u_z \sim \omega^2/\omega_{pe}^2 \sim \omega_{ci}^2/\omega_{pe}^2 \sim (m_e/m_i)^2 (\omega_{ce}^2/\omega_{pe}^2) \sim O(3600^{-2})$,

one obtains $\sigma_s \sim O(.2\, n_z^{4/3})$. In the following sections it will be shown that this value of the surface resistance is generous enough to allow efficient coupling between the antenna and the plasma.

As regards accessibility, the cold-plasma Golant condition (3.1) is not pertinent for the case when coupling occurs directly to the warm plasma. From (3.24) one obtains the warm-plasma accessibility condition

$$n_z > \epsilon_x^{1/2} = O(.1) \tag{3.30}$$

where ϵ_z, σ_i and ν_{ck} are the values occuring at the location of the LHR. This virtually amounts to an unconditional access of the radio-frequency energy into the plasma for frequencys of the order of ω_{ci}.

3.3 E ∥ B_o Gap Coupling

The surface impedance presented by the plasma at a gap (Fig. 2) in the wall is given by

$$\sigma_g = n_{xo}\, \frac{\sigma_s \cos(n_{xo} u_{ca}) - n_{xo} \sin(n_{xo} u_{ca})}{n_{xo} \cos(n_{xo} u_{ca}) + \sigma_s \sin(n_{xo} u_{ca})} \tag{3.31}$$

where $n_{xo}^2 = 1 - n_z^2$ and $u_{xy} = k_o(x-y)$. In obtaining (3.29) it was assumed that only the vacuum waves with the transverse magnetic (TM) polarization are present. The Poynting vector at the plasma surface and the wall losses are, respectively,

$$\mathcal{P} = -\frac{i}{2\eta}\, \frac{\sigma_s |E_o|^2}{|\sigma_s \cos(n_{xo} u_{ca}) - n_{xo} \sin(n_{xo} u_{ca})|^2}, \tag{3.32}$$

and,

$$\mathcal{L} = \frac{1}{2\eta^2 n_{xo}^2} \left| \frac{\sigma_s \sin(n_{xo} u_{ca}) + n_{xo} \cos(n_{xo} u_{ca})}{\sigma_s \cos(n_{xo} u_{ca}) - n_{xo} \sin(n_{xo} u_{ca})} \right|^2 \frac{\rho}{\delta} |E_o|^2, \quad (3.33)$$

where ρ and δ are the specific resistance and skin depth of the wall, respectively and E_o is the n_z Fourier spectrum component excited by the gap. For typical experimental parameters one may readily verify that $|\sigma_g| \sim 1$, i.e. a near perfect match between the gap and the plasma occurs for $n_z \sim 2$. Furthermore $\mathcal{P}/\mathcal{L} \gg 1$ and heating efficiency is close to unity. The gap excitation may be simulated by one of the following approaches:

(i) If the machine dimensions are large enough to accomodate a waveguide of height $h = \lambda_o/2$ in the azimuthal direction, the gap coupling is simulated by a series of waveguides distributed uniformly round the torus and phased so as to give the desired n_z spectrum (PARKER, 1971; KARNEY et al, 1973; LALLIA, 1974).

(ii) Employing a dielectric filled or ridged waveguide allows a reduction in the waveguide height by a factor of up to three (PRIDGEON, 1978). One, however, pays a price of reduced power handling capability for a given access size.

(iii) Since few of the existing machines are large enough to be able to accomodate a waveguide, we suggest using a parallel-plate or coaxial transmission line (Fig. 4) for simulating the gap field. The coaxial waveguide must be properly shaped at the end which includes flaring and flattening the center conductor so as to produce the appearance of a parallel plate line. The problems of this configuration will arise not so much from matching difficulties but from possible breakdown and arcing across to the torus walls. Since this arrangement has no low-frequency cutoff, the advantage as a testbed pending waveguide operation is obvious. As a backup option, the classic loop coupling is described in the following section.

3.5 Loop Coupling

Since the coupling occurs principally from the arm parallel to the plasma surface, the current loop in Fig. 2 may be idealized by a current element J_z. In practice, one would employ a series of such loops distributed uniformly around the torus and phased so as to produce the desired spectrum. Let J_o be the spectrum component associated with n_z. Applying the appropriate boundary conditions $iE_z/H_y = s$ at $x = a$, $\Delta H_y = J_o$ at $x = b$ and $E_z = 0$ at $x = c$, uniquely specifies E_z and H_y in the region $a \leq x \leq c$. One finally obtains the following expressions for the Poynting vector, antenna plus wall losses (treated as a perturbation of the ideal case with a finite conductivity) and the antenna Q ,

$$\mathcal{P} = \frac{1}{2}\eta\, n_{xo}^4\, u_{cb}^2\, \frac{\sigma_{si}}{\sigma_s^2}\, |J_o|^2 , \tag{3.34}$$

$$\mathcal{L} = \frac{\rho}{\delta}\, |J_o|^2 , \tag{3.35}$$

and

$$Q = \frac{\sigma_s^2}{\sigma_{si}\, n_{xo}^2\, u_{cb}} \tag{3.36}$$

where $\sigma_{si} = \mathrm{Im}(\sigma_s)$. In obtaining (3.34) - (3.36) it was assumed that $n_{xo}\, u_{cb} \ll 1$. For this case, as well, $\mathcal{P} \gg \mathcal{L}$ and an efficient coupling occurs. The quality factor $Q \sim O(4)$ and no particular matching difficulties would be encountered.

3.6 Impurity Absorption

Additional cyclotron resonances appear in the plasma in the presence of impurity ion species. As the wave traverses past these singularities it loses part of its energy and suffers an attenuation $\exp(-\Gamma_z)$, where (PURI, 1979)

$$\Gamma_z = \frac{k_o n_x a}{8 \epsilon_x} \left(\frac{\omega_{pi}^*}{\omega_{ci}^*} \right)^2 \frac{e^{-\Lambda^*} I_n(\Lambda^*)}{\Lambda^*}, \qquad (3.37)$$

and the asterik denotes impurity contribution. From (3.24) and (3.26)

$$\Lambda \simeq \frac{1}{2} k_o^2 r_{ck}^2 \left(\frac{-\epsilon_z n_z^2}{\epsilon_x} \right). \qquad (3.38)$$

At the location of the LHR, $\Lambda \sim O(10^{-2})$ and Γ_z in (3.25) is negligibly small. As the wave advances into the plasma Λ increases due to the fast increasing $(-\epsilon_z)$. Ignoring the slower increase in Λ due to r_{ck}^2 and ϵ_x^{-1}, $\Lambda \sim O(1)$ for a density increase of $O(10^2)$ compared to the density at the LHR. This typically occurs for $n_e \lesssim O(10^{12}\text{-}10^{13}\ \text{cm}^{-3})$ quite close to the plasma edge. For $\Lambda \sim O(1)$, $\Gamma_z \sim 1$ for

$$\frac{n_e^*}{n_e} \sim 4\sqrt{2}\, \frac{m_i}{m_e} \frac{v_{ci}}{a} \frac{Z^*}{A^*} \frac{\epsilon_x}{|\epsilon_z|} \frac{\Lambda^* e^{\Lambda^*}}{\Lambda^{1/2} I_n(\Lambda^*)} < 10^{-2} \qquad (3.39)$$

where $n_e^* = Z^* n_i$, the electron contribution from the impurity species. The somewhat sobering implication is that, once the wavelength becomes comparable with the ion-cyclotron radius of the impurity ions, the impurity harmonics become opaque to the radially advancing wave for concentrations of well below one percent.

Thus a prudent recourse would consist in avoiding the presence of impurity harmonics near the plasma edge. One way to accomplish this aim would be to heat at the fundamental tritium cyclotron resonance located near the torus major radius. In this case, since the impurities may be assumed to be sufficiently stripped so that $Z^*/A^* > (1/3)\ (1+A^{-1})$, the wave would encounter no impurity resonances as it travels between the antenna and the major radius.

In contrast to this situation, it would be difficult to avoid O^{VI},

O^{VII} and C^{III} impurity resonances (close to the plasma core) when attempting to heat at the deuterium fundamental resonance. Following cases may occur:

(i) The impurities become fully stripped, their gyrofrequencies coalesce with that of deuterium and their presence is rendered harmless.

(ii) If the heating power is low enough (or conversely the impurity concentration is sufficiently high) so that the heating time constant is of the same order as the energy equipartition time of several tens of microseconds, the impurities act as a relatively harmless intermediaries in the ion heating process.

(iii) The heating power is large (or for very low impruity concentrations), the impurities are rapidly heated and lost from the resonance zone much faster than the replacement time due to diffusion from the surrounding plasma. In such a case majority species heating resumes after an initial power loss to the impurities.

(iv) If,on the other hand, the impurity ions are uncontained and constantly replaced, theyconstitute on energy drain, the precise extent of which can be estimated only by using a transport code in conjunction with the power deposition profile; this being outside the scope of the present undertaking.

Moving up to still higher heating frequencies introduces a host of impurity resonances, some of them uncomfortably close to the plasma edge. Their precise interaction is a matter of detail which for reasons already cited must await either a more ambitious undertaking or direct experimental experience.

3.7 Runaways and the n_z Spectrum

The E_z component inherently associated with the s, p and e waves is extremely effective in accelerating the parallel electron velocities via

ELD. The particle acceleration requires the wave phase velocity $v_p = \omega/kz = c/n_z$ to be equal to the electron thermal speed v_{ze}. Due to the wide spread in the particle velocity, there is always a class of particles resonating with the wave. If the wave too has a large velocity spread (due to a wide n_z spectrum), these particles stay in resonance for a prolonged duration, drawing energy steadily from ever lower n_z components and thereby creating a runaway condition.

Avoidance of runaways has led to ingenious techniques like the deployment of a Faraday shield in blocking out the slow wave component in heating methods using the fast wave coupling. It may, therefore, appear, paradoxical to seek to use the slow-wave coupling scheme for plasma heating. This is a legitimate paradox and special care will have to be exercised in avoiding potentially undesirable runaway scenarios.

From the ELD results for bulk plasma we already know that the damping decreases rapidly with ζ_e as $\zeta_e \exp(-\zeta_e^2)$ and becomes quite small for $\zeta_e \gtrsim 3.5$, principally due to the rapidly decreasing higher energy particle populations in a Maxwellian distribution. Writing,

$$\zeta_e = v_p / v_{ze} = c/n_z v_{ze} \sim 750\, T_e^{-1/2} / n_z , \quad (3.40)$$

one notes that by constraining $n_z \lesssim 2$, ELD is altogether avoidable even in a fully developed thermonuclear plasma. However, since our aim is limited to avoiding the heating near the edge, where $T_e \lesssim O$ (2.5 keV), the less stringent condition $n_z \lesssim 4$ will suffice. Larger values of n_z may be tolerated provided, (i) their energy content is low and (ii) they possess a discrete rather than a continuous spectrum so as to promote a plateau building tendency instead of a continuously fed acceleration leading to runaway heating.

The above considerations would favour a well controlled n_z spectrum created, for example, by appropriately phased and uniformly distributed

gap antennas with a low fundamental n_z so that very little spectral power resides in components with $n_z > 4$.

Since such has not been the case with the antennas hitherto employed in the fast wave coupling experiments, both the necessity of a Faraday shield and the misgivings about the slow wave heating schemes become understandable.

4. BUCHSBAUM HYBRID GROSS BERNSTEIN HEATING

For the case of slow wave coupling from the outer plasma circumference at $\omega_{ci} < \omega < \omega_{ck}$, the cold-plasma singularity $\epsilon_x \to 0$ occurs at the Buchsbaum hybrid resonance (BHR) where $\omega^2 \sim \omega_{ci}\omega_{ck}$ as shown qualitatively in Fig. 1b. Despite close analogy with the LHGB heating there are important differences, namely:

(i) Unlike the lower-hybrid wave, ϵ_x does not monotonically decrease from $\epsilon_x = 1$ at the edge to $\epsilon_x \to 0$ at the resonance. And if the BHR is not located close to the plasma boundary, ϵ_L (along with ϵ_x) may become large enough to allow the presence of the left cutoff $n_z^2 - \epsilon_L = 0$ between the edge and the resonance; introducing evanescence and associated wave reflection. This considerably restricts the choice for the location of the BHR which must be positioned close to the plasma edge to preserve the propagating appearance of Fig. 1b.

(ii) The surface impedance will depend upon the surface conditions in a delicate manner due to large variations in ϵ_x occuring from density fluctuations.

Thus, no particular advantage is to be gained by using this scheme compared to the LHGB wave heating. Apart from the reservations cited above, most of the observations for the LHGB heating are also applicable to this case.

5. FAST WAVE GROSS BERNSTEIN HEATING

5.1 Mode Conversion and Absorption

The Gross-Bernstein electrostatic waves may also be approached by fast wave coupling at the inner torus circumference (JACQUINOT et al., 1977). Following conversion from the fast to the slow wave the wave undergoes further transformations into the plasma and electrostatic modes near the BHR (Fig. 1a). If a sufficiently wide evanescence region separates the confluence from the propagating region on the far side of the Launching antenna, the fast wave would experience complete conversion to the slow mode (ZASLAVSKIJ et al., 1964); this being the case in a plasma consisting of comparable concentrations of the two gas species constituting the hybrid resonance. After the wave conversion, the physics involved is similar to the LHGB heating with the following significant differences of detail:

(i) In the linear model, the wave encounters no ICR of the bulk plasma species so that no direct ion heating appears possible. However, as explained in Sec. 3.6 indirect ion heating via impurity harmonics would, in fact, occur. Since the BHR could be easily located at the major radius, the impurity harmonics would act as a benign presence as far as ion heating is concerned. Further complications leading to partial attenuation of the fast wave at the impurity harmonics (or minority species), prior to the wave conversion at the confluence is treated by SWANSON (1967), PERKINS (1977) and JACQUINOT et al. (1977).

(ii) Unlike LHGB heating, this scheme has withstood the test of successful experimentation both in the TFR (JACQUINOT et al., 1980) and ERASMUS (WEYNANTS et al., 1980) tokamaks.

5.2 Accessibility and Coupling

From Maxwell's equations, the differential equations describing the fast wave propagation near the plasma edge may be written as,

$$\frac{\partial^2 E_y}{\partial x^2} + \frac{(\epsilon_L - n_z^2)}{(\epsilon_x - n_z^2)} (\epsilon_R - n_z^2) E_y = 0 . \quad (5.1)$$

Introducing $\alpha = (\epsilon_L - n_z^2)/(\epsilon_x - n_z^2)$ and $u_c = (\partial \epsilon_R / \partial x)^{-1} (n_z^2 - 1)$, where $u_c = k_o l_c$ and l_c is the distance of the right (magnetosonic)-cutoff from the plasma edge, (5.1) gives

$$\frac{\partial^2 E_y}{\partial x^2} + \alpha (n_z^2 - 1) \frac{\xi}{u_c} E_y = 0 , \quad (5.2)$$

where $\xi = x - u_c$. In (5.2) we treat the slowly varying parameter α as a constant of the order of unity. Proceeding as in Sec. 3.2 and assuming that $u_c n_z \ll 1$ so that the Bessel functions may be approximated by the first term in the series expansion, one obtains from (5.2), the plasma surface impedance

$$\sigma_f = s e^{\pi i/3} u_c^{1/3} \alpha^{-1/3} (n_z^2 - 1)^{-1/3} . \quad (5.3)$$

In order to obtain an estimate of u_c, let us write ϵ_R as,

$$\epsilon_R = 1 + \frac{\omega_{pe}^2}{\omega \omega_{ce}} \left[1 - \frac{f_D}{1 + \frac{\omega}{\omega_{cD}}} - \frac{f_T}{1 + \frac{\omega}{\omega_{cT}}} \right] \quad (5.4)$$

$$= 1 + \frac{\beta}{2} \frac{m_D}{m_e} \frac{\omega_{pe}^2}{\omega_{ce}^2} ,$$

where

$$\beta = \frac{2 \omega_{cD}}{\omega} \left[1 - \frac{f_D}{1 + \frac{\omega}{\omega_{cD}}} - \frac{f_T}{1 + \frac{\omega}{\omega_{cT}}} \right] . \quad (5.5)$$

At the right-cutoff

$$n_z^2 = \epsilon_R = 1 + \frac{\beta}{2} \frac{m_D}{m_e} \frac{\omega_{pe}^2}{\omega_{ce}^2} . \quad (5.6)$$

Writing $u_c/u_a = \omega_{pe}^2/\omega_{po}^2$ where ω_{po} is the electron plasma frequency on the axis (x = 0), (5.6) yields

$$u_c = \frac{2}{\beta} \frac{m_e}{m_D} \left(\frac{\omega_{ce}}{\omega_{po}} \right)^2 (n_z^2 - 1) u_a , \quad (5.7)$$

which together with (5.3) gives,

$$\sigma_f = s\, e^{\pi i/3} \left(\frac{\omega_{ca}}{\omega_{p\bullet}}\right)^{2/3} \left(\frac{m_e}{m_D}\,\frac{2u_a}{\alpha\beta}\right)^{1/3}$$

$$\simeq 0.11\, e^{\pi i/3} \left(\frac{\omega_{ca}}{\omega_{p\bullet}}\right)^{2/3} \left(\frac{u_a}{\alpha\beta}\right)^{1/3} . \qquad (5.8)$$

Note that the approximations $\alpha,\beta \sim O(1)$ are uncritical in the light of one-third power dependence. Also from (5.7), we obtain the justification leading to (5.3). The correct value of ω_{ce} in (5.8) is that near the plasma edge. In the next section we treat the antenna problem for the case of fast wave coupling.

5.3 Loop Coupling

Neglecting the Faraday shield effects and proceeding as in Sec. 3.5, the fast wave loop coupling parameters are

$$P \sim \tfrac{1}{2}\eta \frac{\sigma_{fi}}{(u_{ca}+\sigma_{fr})^2+\sigma_{fi}^2}\, u_{cb}^2\, |J_o|^2 , \qquad (5.9)$$

$$\mathcal{L} \sim \left[1 + \tfrac{1}{2}\left|1 - \frac{u_{cb}}{u_{ca}+\sigma_f}\right|^2\right] \frac{P}{\delta}\, |J_o|^2 , \qquad (5.10)$$

and $$Q \sim \frac{(u_{ca}+u_{fr})^2+\sigma_{fi}^2}{\sigma_{fi}\, u_{cb}} \left[1 - \frac{u_{cb}(u_{ca}+\sigma_{fr})}{(u_{ca}+\sigma_{fr})^2+\sigma_{fi}^2}\right] . \qquad (5.11)$$

In this case too $P \gg \mathcal{L}$ while $Q \sim 0$ (3.5) and excellent efficiency and comfortable matching conditions exist. The loop impedance

$$Z_L = \eta\, u_{cb}\, \frac{l}{w} \left[\frac{u_{cb}\,\sigma_{fi}}{(u_{ca}+\sigma_{fr})^2+\sigma_{fi}^2} + i\left\{1 - \frac{u_{cb}(u_{ca}+\sigma_{fr})}{(u_{ca}+\sigma_{fr})^2+\sigma_{fi}^2}\right\}\right] \qquad (5.12)$$

has convenient values from the experimental standpoint. l and w in (5.12) are the loop height and width respectively.

6. DISCUSSION AND CONCLUSIONS

We have endeavored to present a coherent picture of varied possibili-

ties for coupling to ion Gross-Bernstein waves in a thermonuclear plasma. The models used were deliberately idealized to focus attention on the essential processes involved without loss of pertinent physics. A more complete treatment would consider k_y finite and include such toroidal effects as shear, rotational transform and variations in the n_z spectrum due to toroidicity.

The principal contributions include the derivation of plasma surface impedance both for the slow and fast wave coupling in an analytic form, an estimate of the important role played by the impurities and guidelines concerning the proper choice of the n_z spectrum in order to avoid runaway conditions associated with the slow wave.

Several other allied possibilities for heating at the ICRF, namely, minority heating have not been included in this simple treatment. We draw the reader's attention to the theoretical works of SWANSON (1967) and PERKINS (1977) on this subject.

REFERENCES

BERNSTEIN I.B. (1958) Phys. Rev. 109, 10

BRAMBILLA M. (1976) Nucl. Fusion 16, 47

GOLANT V.E. (1971) Zh. Tekh. Fiz. 41, 2492, (1972) Sov. Phys.-Techn. Phys. 16, 1980

GROSS E.P. (1951) Phys. Rev. 82, 232

JACQUINOT J., MCVEY B.D. and SCHARER J.E. (1977) Phys. Rev. Lett. 39, 88

JACQUINOT J. (1980) Varenna-Grenoble Conference, Como

KARNEY C.F.F., BERS A. and KULP J.L. (1973) Bull. Am. Phys. Soc 18, 1273

LALLIA P., (1974) Proceedings of the Symposium on Plasma Heating in Toroidal Devices (Editrice Compositori, Bologna) p. 120

ONO M. (1979) PPPL-1593, Princeton University

ONO M., STIX T. H. and WONG K.L. (1980a) IAEA, Brussels

ONO M., HORTON R., STIX T.H. and WONG K.L. (1980b) Varenna-Grenoble Conference, Como

ONO M. and WONG K.L. (1980c) Phys. Rev. Lett. 45, 1105

PARKER R.R. (1971) RLE-QPR No. 102, MIT Camb., MA, p. 97

PERKINS F.W. (1977) Nucl. Fusion 17, 1197

PRIDGEON T. (1978) WFPS-TME - 077, Westinghouse Electric Corporation, P.O. Box 10864, Pgn. PA

PURI S. and TUTTER M. (1975) Proceedings of the Second International Conference on Waves and Instabilities in Plasmas (Institute for Theoretical Physics, Innsbruck University), p. P 1

PURI S. (1975) Phys. Letters 55 A, 99

PURI S. (1978) Proceedings of the Third Topical Conference on Radio-Frequency Plasma Heating (California Institute of Technology, Pasadena) p. E3

PURI S. (1979) Phys. Fluids 22, 1716

PURI S. (1980) Varenna-Grenoble Conference, Como

STIX T.H. (1965) Phys. Rev. Lett. 15, 1878.

WEYNANTS R.R., MESSIAEN A.M., LEBLUD C. and VANDENPLAS P.E. (1980) Varenna-Grenoble Conference, Como

ZASLAVSKIJ G.M., MOISEEV S.S. and SAGDEEV R.G. (1964) Akad. Nauk SSR 158, 1295; (1965) Sov. Phys.-Dokl. 9, 863

FIGURE CAPTIONS

Fig. 1 Qualitative dispersion curves for the (a) lower-hybrid, fast-wave and (b) Buchsbaum-hybrid coupling to the electrostatic Gross-Bernstein waves in a toroidal geometry. The hybrid resonances, confluence and cutoffs occur where the cold-plasma coefficients A, $D = B^2 - 4AC$ and C vanish in (2.1)

Fig. 2 Slab geometry describing the idealized antenna configurations. The fast wave loop coupling is assumed to occur at the inner torus circumference. The slow waves, on the other hand, are launched using loops or gaps on the outer torus circumference.

Fig. 3 Computed lower-hybrid wave dispersion characteristics at a fixed ω in the presence of simultaneous density and magnetic field gradients for $T_e = T_i = 100$ eV, $B_o = 60$ kG at the LHR layer marked ω_{LH}. The density is assumed to vary linearly from $n_e = 0$ at the edge to $n_e = n_{LH}$ at the LHR. The solid curve is for ω/ω_{ci} versus log (k_{xr}) and the dotted curves show log (k_{xi}) versus log (k_{xr}). In (a) ω_{LH} occurs at $3.5\,\omega_{ci}$ and in (b) at $1.5\,\omega_{ci}$ while the n_z equals 1.5 and 1.01 for the two cases respectively. In (a) the log (k_{xi}) scale is iterated for $4 \leq \log (k_{xi}) \leq 0$ between each pair of cyclotron harmonics. The lower-hybrid (slow electromagnetic), the plasma and the electrostatic Gross-Bernstein waves bear the labels s, p and e respectively. The curves were obtained for fully ionized deuterium plasma using the complete hot-plasma dielectric tensor description.

Fig. 4 Gap coupling simulation using (a) coaxial line and (b) parallel

plate transmission lines respectively. The center conductor of the coaxial line is assumed to have been flared and flattened at the end to look like a parallel plate line.

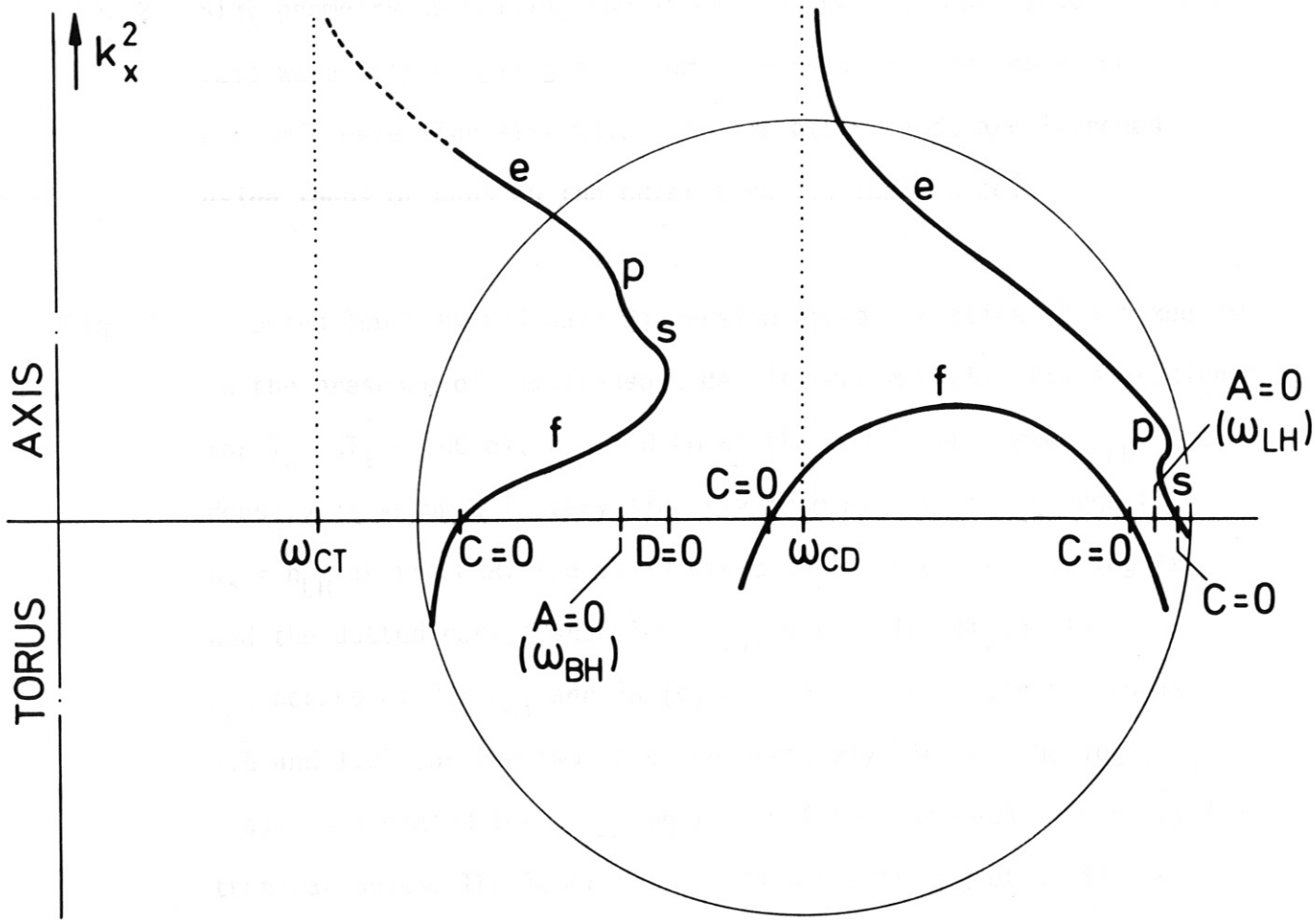
k_x^2
AXIS
TORUS
e
p
s
f
e
f
p
s
A=0
(ω_{LH})
C=0
ω_{CT}
C=0
D=0
ω_{CD}
C=0
C=0
A=0
(ω_{BH})

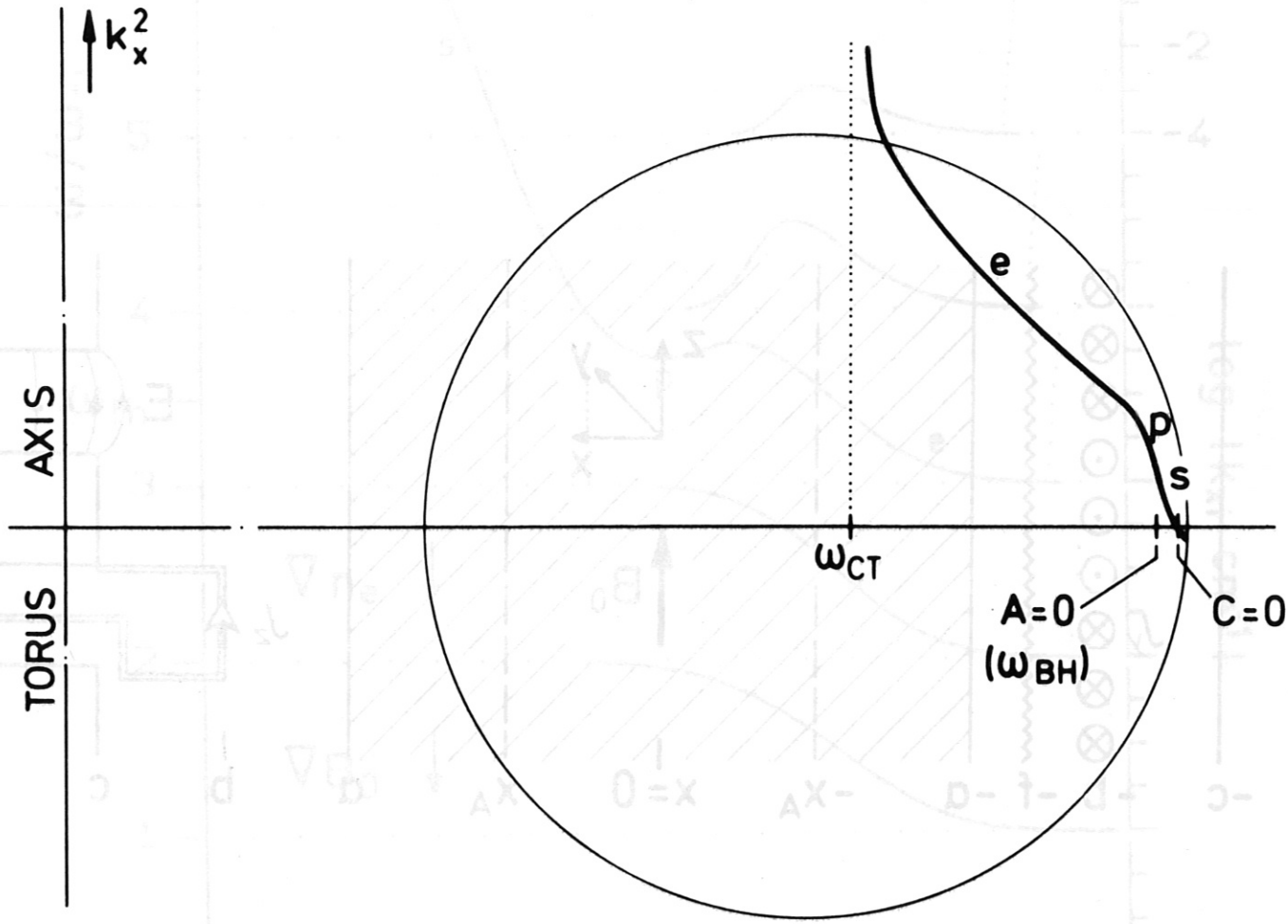
k_x^2
AXIS
TORUS
e
p
s
ω_{CT}
A=0
(ω_{BH})
C=0

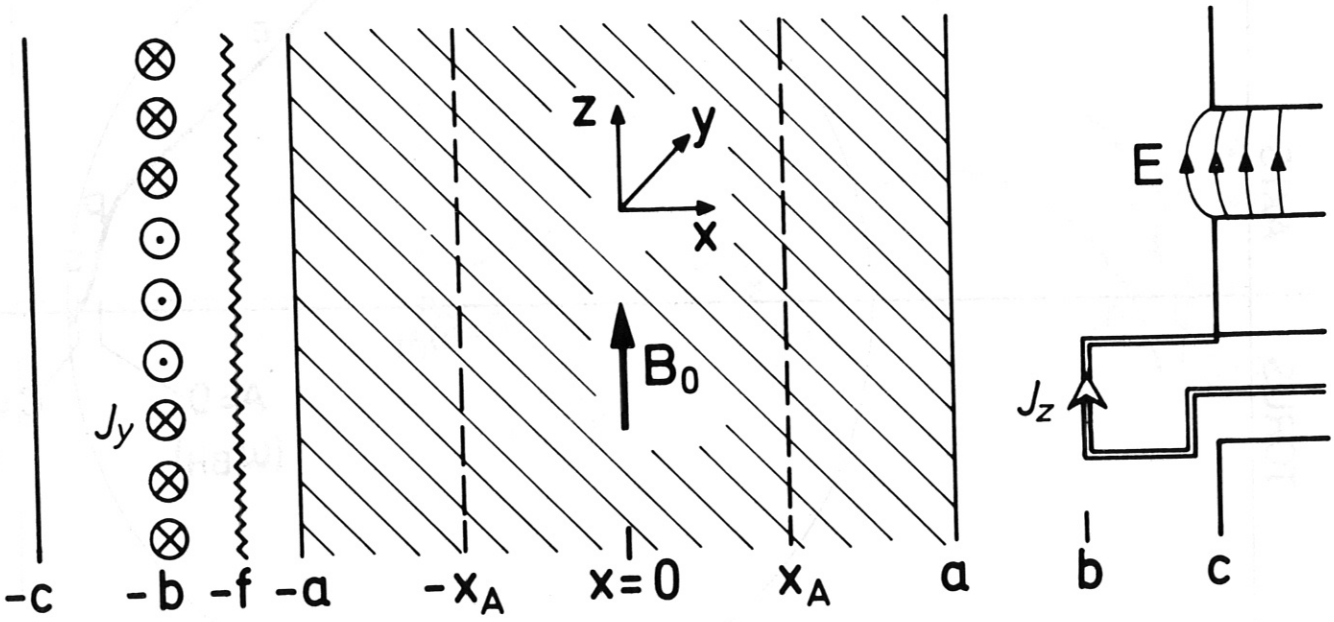
z
y
x
B_0
J_y
-c
-b
-f
-a
$-x_A$
x=0
x_A
a
E
J_z
b
c

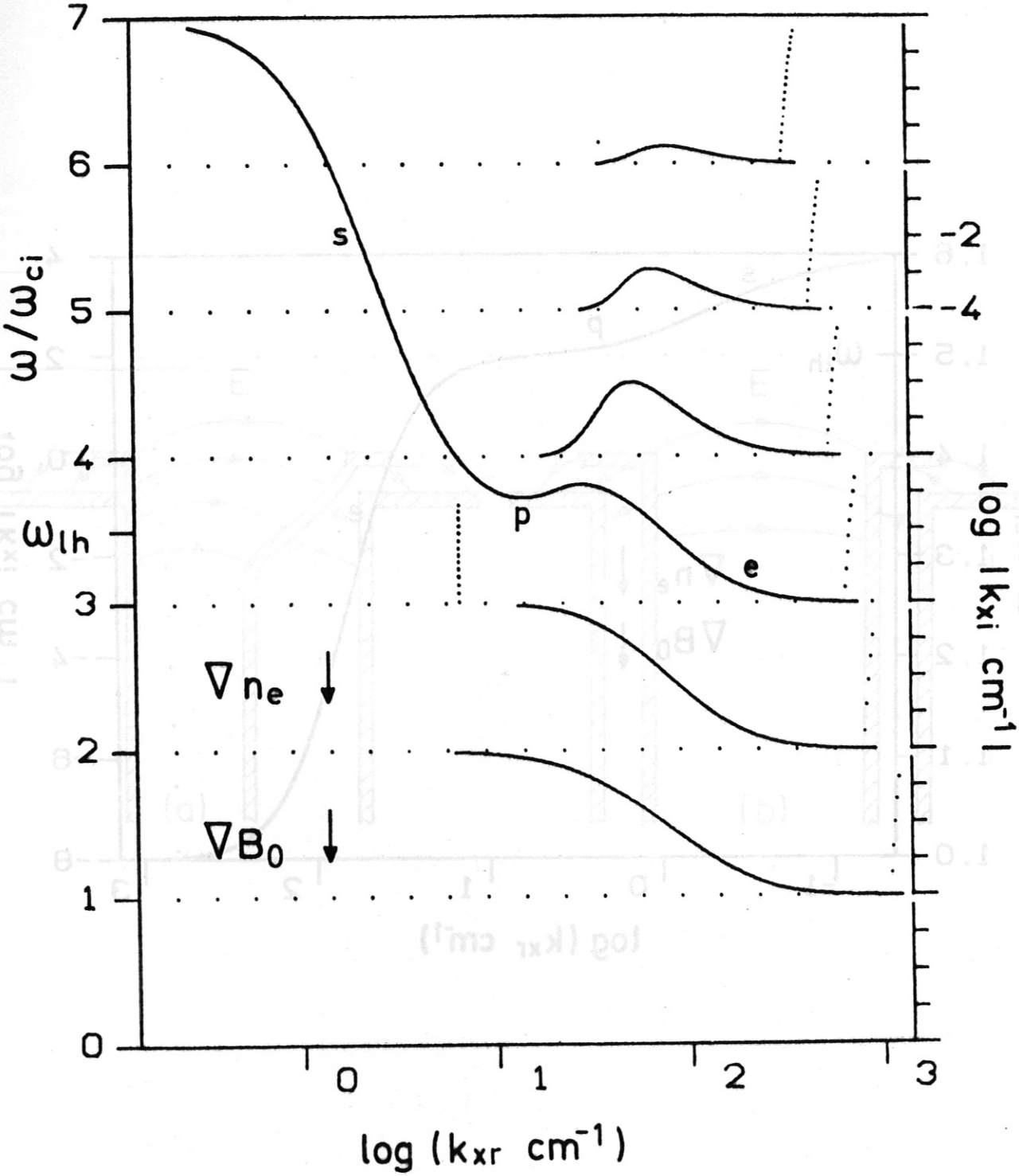
7
6
5
4
3
2
1
0
ω/ω_{ci}
ω_{lh}
s
p
e
∇n_e
∇B_0
-2
-4
log $|k_{xi}$ cm$^{-1}|$
0
1
2
3
log (k_{xr} cm^{-1})

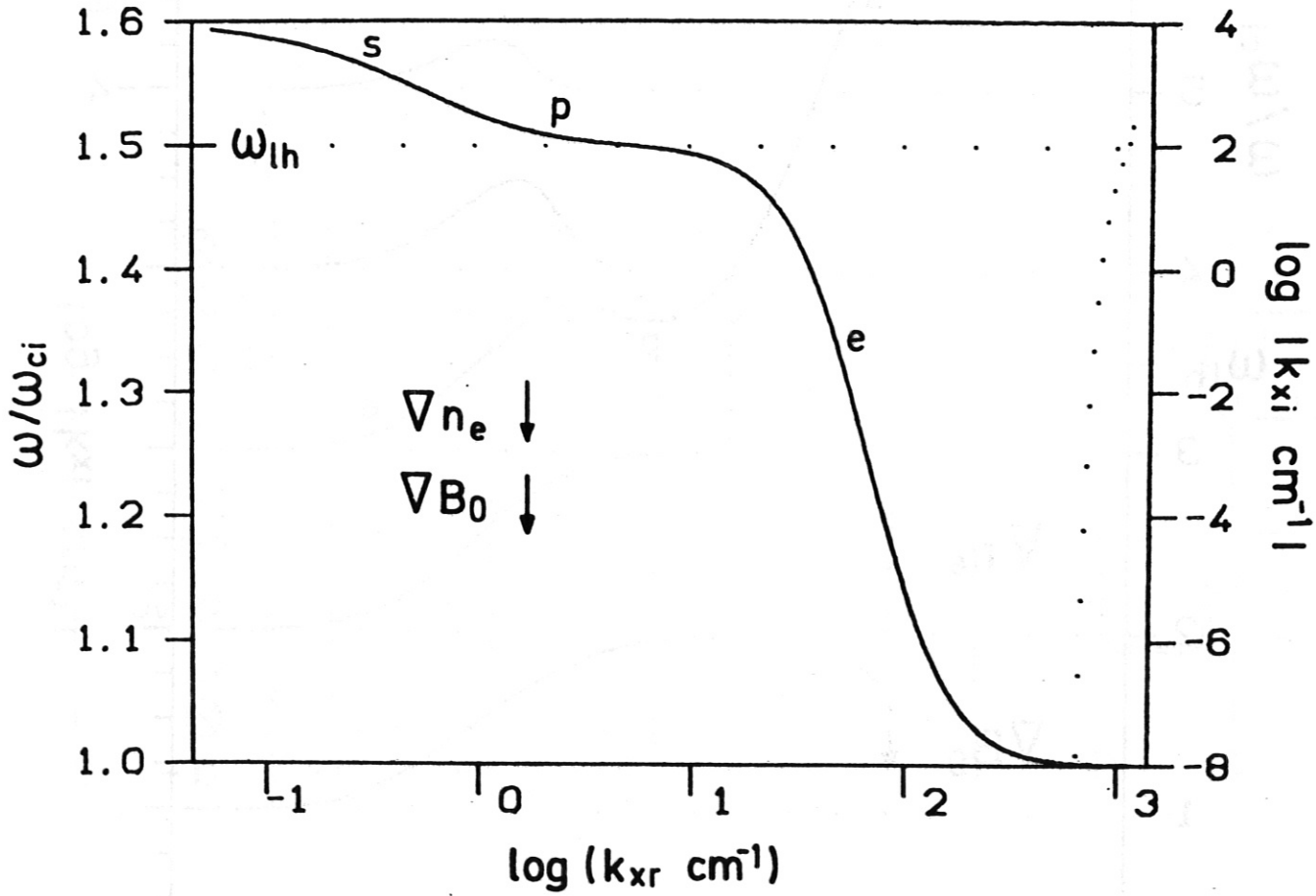
1.6
1.5
1.4
1.3
1.2
1.1
1.0
ω/ωci
s
p
e
ωlh
∇ne
∇B0
-1
0
1
2
3
log (kxr cm-1)
4
2
0
-2
-4
-6
-8
log |kxi cm-1|

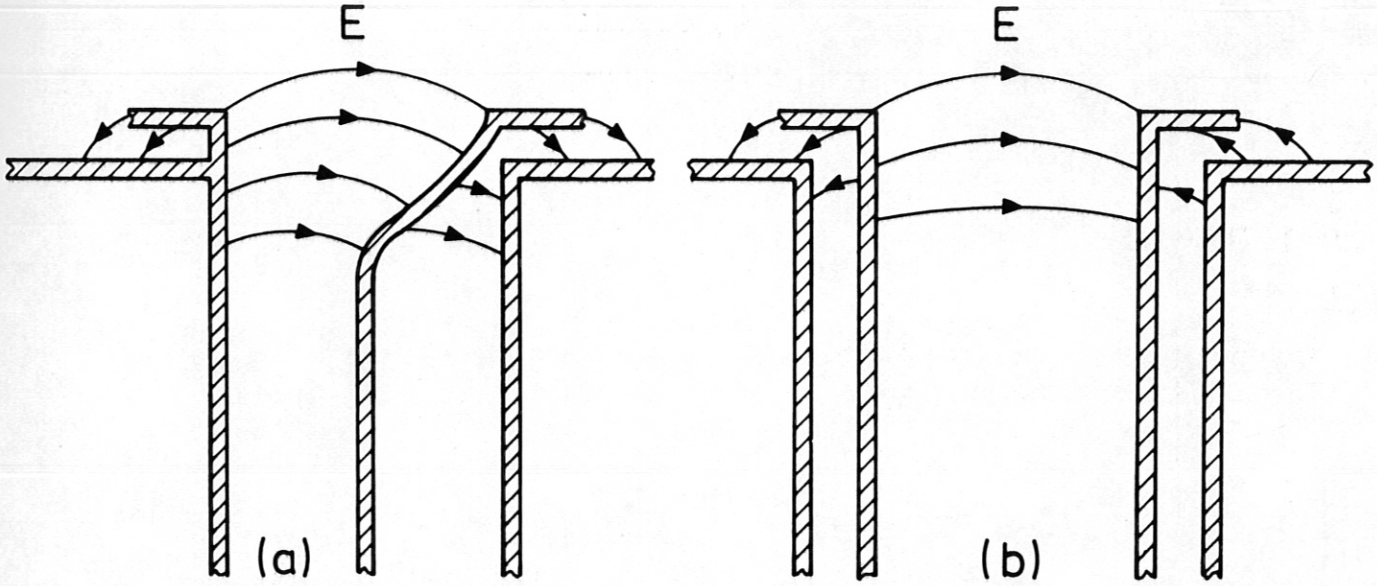
E
E
(a)
(b)